NeuroImage 102 (2014) 345–357

Contents lists available at ScienceDirect

NeuroImage

journal homepage: www.elsevier.com/locate/ynimg

Changes in structural and functional connectivity among resting-state networks across the human lifespan

Richard F. Betzel [a], Lisa Byrge [a], Ye He [b], Joaquín Goñi [a], Xi-Nian Zuo [b], Olaf Sporns [a,*]

[a] Psychological and Brain Sciences, Indiana University, Bloomington, USA
[b] Key Laboratory of Behavioral Science and Magnetic Resonance Imaging Research Center, Institute of Psychology, Chinese Academy of Sciences, Beijing, China

ARTICLE INFO

Article history:
Accepted 31 July 2014
Available online 7 August 2014

Keywords:
Connectome
Functional connectivity
Lifespan
Modularity

ABSTRACT

At rest, the brain's sensorimotor and higher cognitive systems engage in organized patterns of correlated activity forming resting-state networks. An important empirical question is how functional connectivity and structural connectivity within and between resting-state networks change with age. In this study we use network modeling techniques to identify significant changes in network organization across the human lifespan. The results of this study demonstrate that whole-brain functional and structural connectivity both exhibit reorganization with age. On average, functional connections within resting-state networks weaken in magnitude while connections between resting-state networks tend to increase. These changes can be localized to a small subset of functional connections that exhibit systematic changes across the lifespan. Collectively, changes in functional connectivity are also manifest at a system-wide level, as components of the control, default mode, saliency/ventral attention, dorsal attention, and visual networks become less functionally cohesive, as evidenced by decreased component modularity. Paralleling this functional reorganization is a decrease in the density and weight of anatomical white-matter connections. Hub regions are particularly affected by these changes, and the capacity of those regions to communicate with other regions exhibits a lifelong pattern of decline. Finally, the relationship between functional connectivity and structural connectivity also appears to change with age; functional connectivity along multi-step structural paths tends to be stronger in older subjects than in younger subjects. Overall, our analysis points to age-related changes in inter-regional communication unfolding within and between resting-state networks.

Introduction

The brain is a complex system that can be conceptualized as a network of anatomically linked regions and thereby made amenable to analysis using tools from graph theory (Bullmore and Sporns, 2009; Rubinov and Sporns, 2010; Sporns, 2014). The brain's structural connectivity (SC), together with other factors, contributes to shape neurophysiological activity, and thereby influences functional connectivity (FC) among neuronal populations (Wang et al., 2013) and brain regions (Deco et al., 2010; Honey et al., 2009). Whereas SC refers to physical connections between two brain regions, FC is defined as the statistical dependency – e.g. correlation, coherence, mutual information, etc. – between those regions' activity time courses. Graph theoretical analyses of SC/FC networks have revealed a host of non-random attributes, including small-worldness (Achard and Bullmore, 2006; Gong et al., 2009), hubs and cores (Achard et al., 2006; Hagmann et al., 2008; Zuo et al., 2012), a structural rich club (van den Heuvel and Sporns, 2011), modular architecture (Meunier et al., 2009, 2010; Betzel et al., 2013), and economic wiring (Bassett et al., 2010; Bullmore and Sporns, 2012), among others.

Resting brain FC can be decomposed into resting-state networks (RSNs) composed of brain regions that exhibit coherent activity in a task-free state (Buckner et al., 2013), exhibit consistent spatial topographic patterns across the cerebral cortex (Power et al., 2011; Yeo et al., 2011), and strongly resemble collections of brain regions corresponding to task-evoked sensory, motor and higher-order cognitive systems (Crossley et al., 2013; Smith et al., 2009). RSNs can be extracted using different methodologies, including independent component analysis (ICA; Beckmann et al., 2005) and clustering approaches applied to whole-brain FC networks (e.g., Bellec et al., 2010; Power et al., 2011; Yeo et al., 2011). A number of recent studies have focused on changes in connectivity within and between RSNs, both on fast time scales in the course of spontaneous brain dynamics (Allen et al., 2014; see Hutchinson et al., 2013 for a systematic review), as well as in the course of visual perceptual learning (Lewis et al., 2009), acquisition of motor skills (Ma et al., 2011) and cognitive practice (Jolles et al., 2013).

This report aims to characterize changes in the pattern of SC/FC over the course of the human lifespan, with a focus on connectivity changes within and between RSNs. A number of previous studies have shown that patterns of SC/FC undergo characteristic changes over developmental stages and aging (Cao et al., 2014; Wang et al., 2012; Yang et al.,

* Corresponding author.
E-mail address: osporns@indiana.edu (O. Sporns).

http://dx.doi.org/10.1016/j.neuroimage.2014.07.067
1053-8119/

2014; Zuo et al., 2010). In childhood, FC is dominated by short-range local links, which are gradually replaced by long-distance functional connections in adulthood, forming mature RSNs (Fair et al., 2009; Kelly et al., 2009; Power et al., 2011; Supekar et al., 2010). In contrast, aging studies have demonstrated the opposite effect, with RSNs exhibiting decreased FC (Andrews-Hanna et al., 2007; Ferreira and Busatto, 2013; Geerlings et al., 2014). Studies of SC across the lifespan have demonstrated that hub regions and modules are present by early childhood, though changes of cortical white-matter connectivity continues across the lifespan (Gong et al., 2009; Hagmann et al., 2010; Lim et al., 2013).

While these studies and others have provided insight into the development and maturation of specific RSNs (e.g. Fair et al. (2007, 2008, 2009) for control networks and Andrews-Hanna et al. (2007) for the default mode and dorsal attention networks), few reports have examined age-related changes in connectivity at the whole-brain level across the entire lifespan. Moreover, studies that focus on the intrinsic connectivity of a specific RSN necessarily overlook any connections that that RSN makes to the rest of the brain and how these connections change as a function of age. Here, we aim to bridge this particular gap in knowledge by tracking the age-related change in all functional and structural connections in the human brain over the course of the lifespan. Because RSNs are thought to correspond to the brain's functional systems, it was of particular interest to observe how these changes were related to the boundaries of RSNs and their distributed subcomponents. An additional aim was to gain insight into how changes in SC and FC might be interrelated, and what these changes might reveal about age-related changes in interregional communication.

Methods and materials

NKI-RS lifespan sample and image preprocessing

Lifespan data used in this study are part of the publicly available NKI-Rockland Sample (http://fcon_1000.projects.nitrc.org/indi/pro/nki.html) from the Nathan Kline Institute (NKI, NY, USA) consisting of $N = 126$ subjects (58 female) over the age range 7–85 years (median age = 31.5). The study was approved by the NKI institutional review board and all adult and child subjects provided informed consent (Nooner et al., 2012).

Subjects in this study underwent a scan session using a Siemens TrioTM 3.0 T MRI scanner. Resting fMRI scans were collected using an echo-planar imaging (EPI) sequence with the following parameters: time repetition (TR) / time echo (TE) = 2500 / 30 ms, flip angle (FA) = 80°, field of view (FOV) = 216 × 216 mm^2, voxel size = 3.0 × 3.0 × 3.0 mm^2, distance factor = 10%, number of slices = 38. Each scan session was 650 s long and comprised 260 functional volumes. Inside the scanner, subjects received instructions to keep their eyes closed, relax their minds, and to not move. T1-weighted images were acquired using the following magnetization-prepared rapid gradient echo (MPRAGE) sequence: TR / TE = 2500 / 30 ms, inversion time = 1200 ms, FA = 8°, FOV = 256 × 256 mm^2, voxel size = 1.0 × 1.0 × 1.0 mm^3, number of slices = 192. T1-weighted images were subsequently used for spatial normalization and group-specific template generation.

This sample has been used in two recent studies on the human brain functional connectivity changes across the lifespan (Cao et al., 2014; Yang et al., 2014). The Connectome Computation System (CCS: http://lfcd.psych.ac.cn/ccs.html) was used to preprocess both R-fMRI and DTI images for subsequent analyses. As in Cao et al. (2014), preprocessing of functional images included discarding the first four EPI volumes to allow for the signal to reach equilibrium, correction for timing offsets, 3D geometrical displacement correction for head motion, and 4D global mean-based intensity correction. Motion correction was performed using the Friston-24 model, which regresses out nuisance parameters including six head motion parameters, those same parameters at the previous time step, and both sets of parameters squared (Friston et al., 1996). Additionally, global mean, white matter, and cerebrospinal fluid signals were also included as nuisance parameters and regressed out. Lastly, the signal was band-pass filtered (0.01–0.1 Hz) and both linear and quadratic trends removed.

The preprocessing steps of DTI images are identical to those used in an earlier study (van den Heuvel and Sporns, 2011). Specifically, DTI images were corrected for eddy-current distortions and realigned to the mean image of the 12 unweighted B0 images (Andersson and Skare, 2002). Using the corrected DTI data, a tensor was fit to the diffusion profile within each voxel and the diffusion direction within each voxel was assigned as the principal eigenvector of the tensor by computing its eigen-system (Chang et al., 2005). To provide information on the diffusion direction within a given voxel, its fractional anisotropy (FA) was computed as the square root of the sum of squares (SRSS) of the diffusivity differences, divided by the SRSS of the diffusivities. Using the information on preferred diffusion direction with each voxel in the whole brain mask, the white matter tracts were reconstructed with FACT (fiber assignment by continuous tracking) algorithm (Mori and van Zilj, 2002; Mori et al., 1999). Specifically, within each voxel, evenly distributed 32 seeds were used as starting points of possible streamlines, which generate the white matter fibers by following the preferred diffusion direction from voxel to voxel. A threshold on FA of 0.1 or a sharp turn of >45° was set to stop tracking a fiber streamline at a voxel.

Construction of FC networks

In order to address questions related to RSNs, we used a previously established functional parcellation of the human cerebral cortex (Yeo et al., 2011). This particular parcellation was derived by clustering the whole-brain functional connectivity networks of 500 subjects (along with a 500 subject replication cohort) according to the similarity of regions' functional connectivity profiles. This procedure resulted in seven clusters, whose boundaries shared a close correspondence to the known topographic boundaries of visual (Vis) and somatomotor (SomMot) networks, limbic regions (Limbic) and distributed association networks for executive control (Cont), attention (DorsAttn, SalVentAttn), and internally-directed cognition (Default). These seven RSNs displayed hierarchical organization such that each of the seven clusters could be subdivided into components with distinct patterns of FC, resulting in a total of 17 RSN components or sub-networks: VisCent, VisPeri, SomMotA, SomMotB, LimbicA, LimbicB, ContA, ContB, ContC, DorsAttnA, DorsAttnB, SalVentAttnA, SalVentAttnB, DefaultA, DefaultB, DefaultC, and DefaultD. Across all the 17 sub-networks, there are in total $n = 114$ separated anatomical regions of interest (ROIs). Specifically, any of the ROIs meets two basic requirements: 1) it is isolated anatomically from other regions within the sub-network it belongs to, and 2) is separated by the network boundaries from regions within other sub-networks. These ROIs were then used to represent nodes in both FC and SC networks. The functional connection between nodes i and j was defined as the Fisher-z transformed Pearson product–moment correlation of the representative BOLD time series recorded at those nodes. In the standard surface space defined by FreeSurfer (i.e., *fsaverage5*), representative time series were computed as the average time series of all voxels within an ROI extracted from the transformed individual preprocessed R-fMRI data on the *fsaverage5* surfaces (Jiang et al., 2014). For each subject, FC between all pairs was organized into an $n \times n$ weighted and signed correlation matrix, A^{FC}, whose elements a_{ij}^{FC} denoted the FC between nodes i and j. It is common practice to sparsify A^{FC} by retaining only a fraction of the strongest connections or entries that survive a threshold for statistical significance (Achard and Bullmore, 2006; Cao et al., 2014). In this study FC networks were not sparsified. Eliminating connections impairs our ability to assess how FC changes with age — removing a connection from some subjects but not from others results in fewer observations and a reduction in statistical power. A group-averaged FC matrix (for visualization only) representing all subjects is shown in Fig. 2A. (See Fig. 1.)

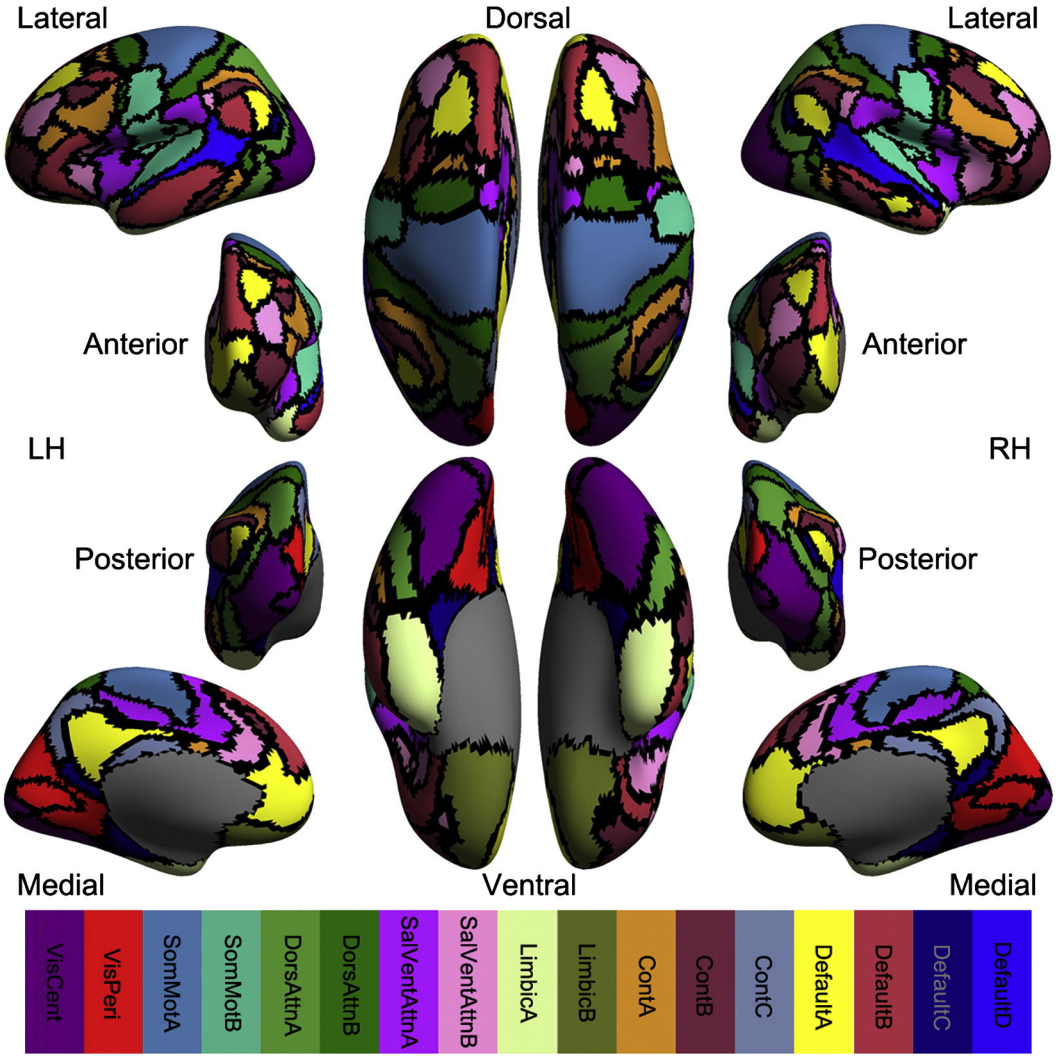

Fig. 1. Surface rendering of all 17 RSN sub-networks comprising 114 brain regions in total onto both left hemisphere (LH) and right hemisphere (RH). The inflated surfaces are provided by FreeSurfer (*fsaverage*). The cortex is divided into 17 components derived from a total of 7 RSNs (Yeo et al., 2011): control components A, B, and C (ContA, ContB, ContC); default mode components A, B, C, and D (DefaultA, DefaultB, DefaultC, DefaultD); dorsal attention components A, B (DorsAttnA, DorsAttnB); limbic components A, B (LimbicA, LimbicB); saliency/ventral attention components A, B (SalVentAttnA, SalVentAttnB); somatomotor components A, B (SomMotA, SomMotB); visual central (VisCent) and peripheral (VisPeri) components. The colormap indicates colors picturing each of the 17 components and their regions on the surfaces.

Construction of SC networks

SC was measured between the same $n = 114$ cortical ROIs used to define nodes in FC networks. Deterministic fiber tracking was performed as in a previous work (van den Heuvel and Sporns, 2011) except that 32 seeds were started in each voxel. The fiber tracking procedure yielded matrices NF_{ij} and FA_{ij} whose elements represented the number of reconstructed fibers connecting nodes i and j and the average fractional anisotropy of completed fiber tracts, respectively. We considered nodes i and j to be adjacent if they were connected by at least one fiber tract. For each subject, the full set of connected nodes was encoded in a binary adjacency matrix, A^{bin}, whose elements a_{ij}^{bin} were equal to 1 if i and j were connected and zero, otherwise. Each pair of connected nodes was also assigned a weight based on NF_{ij} and FA_{ij}. The set of connection weights were stored in the matrix, A^{wei} and were calculated according to the expression:

$$a_{ij}^{wei} = FA_{ij} \times NF_{ij}^{\gamma}$$

where γ acts like a soft threshold on the matrix NF_{ij} (Lohse et al., 2013; Schwarz and McGonigle, 2011; Zhang and Horvath, 2005). Only when $\gamma = 0$, do the elements of NF_{ij}^{γ} become binary variables and edge weights $a_{ij}^{wei} = FA_{ij}$. For $\gamma > 0$, the elements of NF_{ij} contribute to determining the weight of structural connections. In this manuscript we explored eleven possible values of γ equally spaced over the interval [0, 2]. The lower bound was selected because $\gamma < 0$ tends to reward nodes connected by a smaller number of fibers with a stronger edge weight. The upper bound was selected because for $\gamma > 2$, the resulting SC matrix tends to be dominated by one or two strong edges. Both of these particular regimes seem biologically unrealistic. A group-averaged SC matrix evaluated at $\gamma = 0.6$ is shown in Fig. 2B. We would like to note that we explored other schemes for assigning the weight of a structural connection including some that incorporate a correction based on ROI size (e.g. by dividing a_{ij}^{wei} by $V_i + V_j$, where V_i is the size, in number of voxels, of region i). In general, our results are robust to size-corrected weighting schemes. Consequently, all subsequent analyses were performed on SC matrices, A^{wei}, where the edge weights were uncorrected for ROI size.

Multiple linear regression analysis

In general, we were interested in how some variable, y, which might represent the magnitude of a connection weight or the value of some graph-theoretic measurement, changes over the lifespan. Typically y is

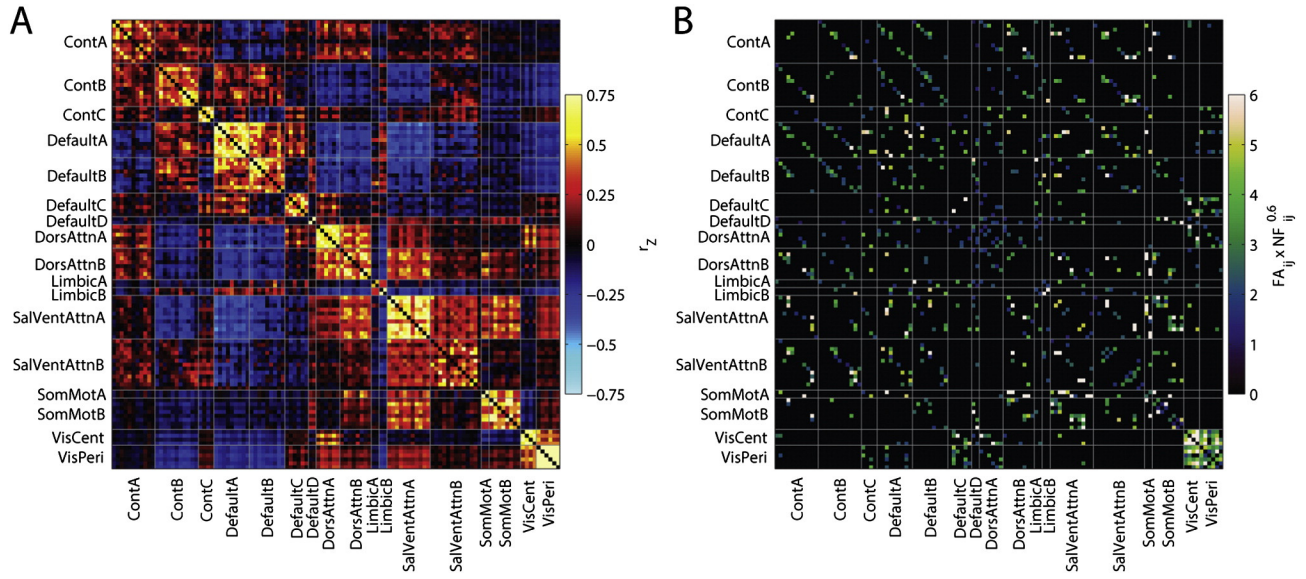

Fig. 2. Group-averaged (all ages) FC (A) and SC (B) organized according to RSN components. This particular SC matrix was generated by setting $\gamma = 0.6$. In panel B, the SC matrix, a connection is shown only if it was present in at least one quarter (32) of all participants.

defined for all subjects such that we can create a $[N \times 1]$ vector of those values, which we denote $\mathbf{y}$. To model y over the lifespan, we made use of multiple linear regression (MLR) models, which have the standard form:

$$\hat{\mathbf{y}} = \mathbf{X} \cdot \beta_{\mathbf{X}} + \mathbf{G} \cdot \beta_{\mathbf{G}} + \mathbf{e}.$$

Here, $\hat{\mathbf{y}}$ is an $[N \times 1]$ vector of estimations of y, the variable of interest, $\mathbf{X}$ is the design matrix with associated parameters $\beta_{\mathbf{X}}$, $\mathbf{G}$ is an $[N \times 3]$ matrix of nuisance variables (gender, total intracranial volume, and mean frame-wise displacement) with the associated $[3 \times 1]$ vector of nuisance parameters $\beta_{\mathbf{G}}$, and $\mathbf{e}$ is an $[N \times 1]$ vector of error terms. The size of $\mathbf{X}$ and $\beta_{\mathbf{X}}$ was dependent on the choice of design matrix, of which we explored two possibilities, corresponding to linear and quadratic models, respectively:

$$\mathbf{X}_{[N\times 2]} = \begin{bmatrix} 1 & age_1 \\ \vdots & \vdots \\ 1 & age_N \end{bmatrix} \quad \text{with} \quad \beta_{\mathbf{X}} = [\beta_0 \quad \beta_1]$$

$$\mathbf{X}_{[N\times 3]} = \begin{bmatrix} 1 & age_1 & age_1^2 \\ \vdots & \vdots & \vdots \\ 1 & age_N & age_N^2 \end{bmatrix} \quad \text{with} \quad \beta_{\mathbf{X}} = [\beta_0 \quad \beta_1 \quad \beta_2]$$

The model that best described the lifespan trajectory of $\mathbf{y}$ was selected as the one with a smaller Akaike information criterion (AIC) value, representing a tradeoff between model likelihood and complexity.

The parameters $\beta_{\mathbf{X}}$ were used to ascertain whether or not a model exhibited a statistically significant age effect. One-sample t-tests were performed on the β associated with the highest order age term (β_1 if the model is linear; β_2 if the model is quadratic). A model was said to exhibit a statistically significant age effect if the p-value associated with that test was smaller than a critical value, p_{crit}. In general, $p_{crit} = 0.01$. In the cases where it was necessary to correct for multiple comparisons, p_{crit} was adjusted using the linear step-up procedure for controlling the false discovery rate (FDR; $q < 0.01$) (Benjamini and Hochberg, 1995).

It should be noted that the nuisance variable "mean frame-wise displacement" was estimated based on subjects' motion during the resting fMRI scan. While the effect of motion on FC has been well-documented (see Power et al., 2012, 2014) potential effects of subject motion on diffusion-weighted images and tractography algorithms are less understood. Consequently, it is unclear whether it is appropriate to include the motion parameter as a nuisance variable in a MLR model. Therefore, in all cases where MLR models were fit to SC data, we tried models that included framewise displacement as a nuisance variable as well as models that excluded it. All results reported in subsequent sections are independent of this decision.

FC edge trajectories

The first series of analyses focused on characterizing age-related changes in FC. To assess whether there were global trends in FC across the lifespan, we separately modeled the average FC within and between RSN components using MLR models. To further quantify age-related change at a finer scale, MLR models were also fit to the functional connections between every pair of nodes, i and j.

FC modularity analysis

In addition to modeling edge-level changes in FC, we also analyzed system-level properties of FC networks using tools from graph theory. Of particular interest was whether the cohesiveness of RSNs changed over the lifespan. Cohesiveness, in this case, refers to a high magnitude of internal FC and weak external FC. This conceptualization of cohesiveness is consistent with the definition of the graph-theoretic measure, "modularity." Modularity quantifies the extent to which a network can be decomposed into internally integrated, yet globally segregated communities (Newman, 2006). For weighted and signed networks like FC, modularity can be calculated as $Q^* = \sum_c q_c^*$, where q_c^* is the contribution to Q^* by a community c and is defined as:

$$q_c^* = \frac{1}{m^+}\sum_{ij\in c}\left[a_{ij}^+ - \frac{s_i^+ s_j^+}{2m^+}\right] - \frac{1}{m^+ + m^-}\sum_{ij\in c}\left[a_{ij}^- - \frac{s_i^- s_j^-}{2m^-}\right]$$

In this expression, $a_{ij}^{\pm}$ contains either the positive or negative edge weights of a_{ij}^{FC} The variables $m^{\pm} = \frac{1}{2}\sum_{ij} a_{ij}^{\pm}$ and $s_i^{\pm} = \sum_j a_{ij}^{\pm}$ are the signed weight of the entire network and node strength, respectively (Rubinov and Sporns, 2011). Each RSN was regarded as a community, and its modularity contribution, q_{RSN}^*, was calculated. In order to quantify changes in the modularity of RSN components across the human lifespan, MLR models were fit to the lifespan trajectory of each of the 17 RSN components' modularity contributions, q_{RSN}^*, according to the procedure described earlier.

SC measures and hubs

We characterized SC matrices with three variables: the total number of binary connections, $m = \frac{1}{2}\sum_{ij} a_{ij}^{bin}$; the total number of streamlines, $nf = \frac{1}{2}\sum_{ij} NF_{ij}$; and the average FA of all edges, $fa = \frac{1}{2m}\sum_{ij} FA_{ij}$.

We also identified highly connected, highly central hub regions following an analysis of both binary and weighted versions of SC networks. Analysis of binary networks consisted of measuring each node's total number of connections (degree), $k_i = \sum_j a_{ij}^{bin}$, and each node's local efficiency, $e_i = \frac{1}{n-1}\sum_{j\neq i} d_{ij}^{-1}$, where d_{ij} is the length of the shortest path connecting nodes i and j. Analysis of weighted networks consisted of several node-wise measures, including node strength, $s_i = \sum_j a_{ij}^{wei}$ and betweenness centrality, b_i, which measures the number of shortest paths traversing a given node.

We defined a region's "hubness" as its average rank across node degree (k_i), node strength (s_i), nodal efficiency (e_i), and betweenness centrality (b_i), estimated from each participant's SC matrices and averaged across all participants. Hubs were defined as the regions with the top-ranked aggregate hub scores. We chose this composite definition of hubness based on the fact that no single metric unambiguously qualifies a node as a hub — e.g. a high degree node may form only weak connections (low strength) or have small betweenness centrality. By assigning each node a composite hub score based on many different measures, we ensure that the nodes we label as hubs score high across several different graph metrics.

Path efficiency framework

SC networks enable distant brain regions to communicate with one another, and hence an important question concerns the effect of age on communication efficiency. To address this question, we defined a measure of path efficiency that could be quantified for every pair of nodes, and then modeled its trajectory across the lifespan. The path efficiency between nodes i and j is closely related to the total weight of the shortest weighted path connecting those nodes. Intuitively, if the shortest path involves few steps and is composed of edges with large weights, then the efficiency of that shortest path should be large. Conversely, shortest weighted paths that involve many steps and weak edges are, intuitively, less efficient. This notion of efficiency is captured by first transforming edge weights from measuring the strength of association to measuring distance, which was accomplished by the simple inversion, $\frac{1}{a_{ij}^{wei}}$, which ensures that nodes connected by strong edges are "closer" to one another than nodes connected by weak edges. Following this inversion, the total weight of the shortest path was calculated using Dijkstra's algorithm (Dijkstra, 1959). Calculating the shortest weighted path between every pair of nodes defines two matrices, D^{wei} and D^{steps}, whose elements d_{ij}^{wei} and d_{ij}^{steps} were equal to the total weight of the shortest weighted path and the length (in discrete steps) of that path, respectively. Finally, to convert weight into efficiency, D^{wei} was inverted in an element-wise fashion and transformed into the efficiency matrix, E^{wei}, whose elements were equal to $e_{ij}^{wei} = \frac{1}{d_{ij}^{wei}}$ (Latora and Marchiori, 2001). Thus, the elements of E^{wei} represent the efficiencies of the shortest weighted path between any two nodes. In order to quantify changes in efficiency across the human lifespan, the trajectory of path efficiency between each pair of nodes was modeled using the same MLR procedure described earlier but without mean frame-wise displacement included as a nuisance variable.

FC distance dependence

The final analysis of SC builds on the previous section. We hypothesized that changes in the topology of SC over the lifespan would have an impact on the capacity of SC for routing information, a change that might be manifested in FC. For example, nodes that early in life had been connected by efficient paths comprising few processing steps and strong edges may rely on less efficient, multi-step communication strategies later in life. To address whether the length of shortest paths influenced FC and whether this relationship changed over the lifespan, we examined the matrices, D^{steps}, which measured the number of steps in the shortest weighted paths connecting all pairs of nodes. For each subject, we computed the average FC of edges connected by $d_{ij}^{steps} = 1, 2, 3, \ldots$. Then, for each number of steps we asked how the average FC at that distance was correlated with age across all subjects. This analysis, along with the other analyses of structural connectivity, was carried out at all levels of γ.

All analyses were run in Matlab (The Mathworks, Inc., Natick, MA, USA). Graph theoretical analysis was performed using custom software as well as software made available as part of the Brain Connectivity Toolbox (https://sites.google.com/site/bctnet/; Rubinov and Sporns, 2010).

Results

FC decreases within RSNs and tends to increase between RSNs

MLR models were fit to the average FC within and between RSN components, which revealed that, on average, FC within RSNs decreased with age, while the opposite was true of FC between RSNs. Both models were statistically significant ($p < 0.01$, uncorrected) (Fig. 3). This figure suggests that, on average, functional connections within RSNs follow decreasing trajectories with age while connections between RSNs increase in magnitude. An important question is whether these changes are driven by specific functional connections/RSNs.

In order to assess whether FC between specific regions (nodes) exhibited age-related change, MLRs were fit to lifespan trajectories of the $n_c = \frac{114\times113}{2} = 6441$ functional connections. This analysis revealed 85 functional connections that exhibited statistically significant age-related change, representing 1.3% of all possible edge comparisons ($q < 0.01$, FDR-corrected; corresponding to an uncorrected $p = 1.3 \times 10^{-4}$) (Fig. 4). These edges involved only 60 of the possible 114 cortical regions (nodes) and represented 15 of the 17 RSN components (DefaultC and LimbicB were not represented). The interregional distances of the 85 statistically significant edges ranged from 9 mm to 130 mm. To assess whether interregional distance was systematically related to the likelihood of an edge exhibiting a statistically significant age effect, we calculated the Spearman correlation of interregional distance with the corresponding p-value. We performed this calculation with all edges grouped together and for linear and quadratic models separately. If there was a bias towards either long- or short-range connections exhibiting an age-related effect, we would expect this correlation to be non-zero. In all cases, we found no clear relationship of p-value to interregional distance: $r_{all} = 0.0068$, $r_{linear} = -0.03$, $r_{qudratic} = 0.058$. A complete description of all statistically significant models and their parameters can be found in SI Table 1. Figs. 5A and B depict FC versus age trajectories for select edges within and between RSN components, respectively.

Of the 85 connections exhibiting statistically significant age effects, 22 connected nodes that belonged to the same RSN component. Ten of these connections exhibited lifespan trajectories that were best described by linear decreases with respect to age and included regions representing ContC (precuneus, posterior cingulate), DefaultB (anterior temporal lobe, dorsal prefrontal, inferior parietal lobule), ContA (lateral prefrontal, anterior cingulate), VisPeri (inferior extrastriate), and SalVentAttnB (medial posterior prefrontal). The ten linearly decreasing functional connections were positively coupled early in life and included edges that were among the strongest in the entire network, with mean FC at age 7 of 0.69 ± 0.44. With age, FC between these regions is predicted to become less positive, with a mean change in FC from

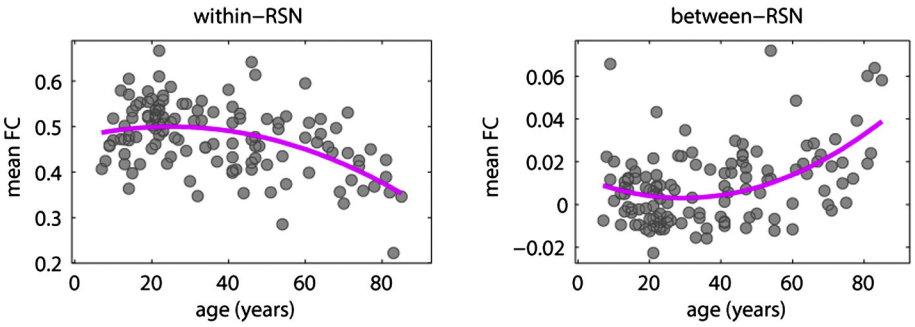

Fig. 3. Age-related changes in average FC within (left) and between (right) RSN components. Both trajectories are statistically significant at $p < 0.01$.

age 7 to 85 of -0.37 ± 0.05. Because these connections were initially very strong, this decrease in FC magnitude served only to make them less strong, rather than weaken them to the point that their FC approached zero.

The lifespan trajectories of the remaining twelve within-component connections were best fit by convex quadratic models and involved regions from SalVentAttnA (ventral pre-central, insular, medial parietal, medial frontal), VisCent (striate), and SomMotB (insula, secondary somatosensory). FC of these edges was of modest magnitude early in life (mean FC of 0.36 ± 0.19 at age 7), but doubles by the time they reach their respective peaks (mean peak FC of 0.74 ± 0.19; mean peak age of 40.9 ± 5.4 years, where peak age was computed as $\frac{-\beta_1}{2\beta_2}$). At age 85 the average FC of these edges decreases to a magnitude less than the magnitude of FC at age 7 (mean FC at age 85 is 0.18 ± 0.13), meaning that on average, these regions exhibit decreased FC over the entire lifespan.

The remaining 63 edges fell between RSN components. Among the models describing these edges 9 were linear-decreasing, 19 were linear-increasing, 19 were quadratic-convex, and 16 were quadratic-concave. These models were more variable in terms of their predictions for FC changes across the lifespan (36 predict increases; 26 predict decreases), though the net change in FC from age 7 to 85 was 0.07 ± 0.24.

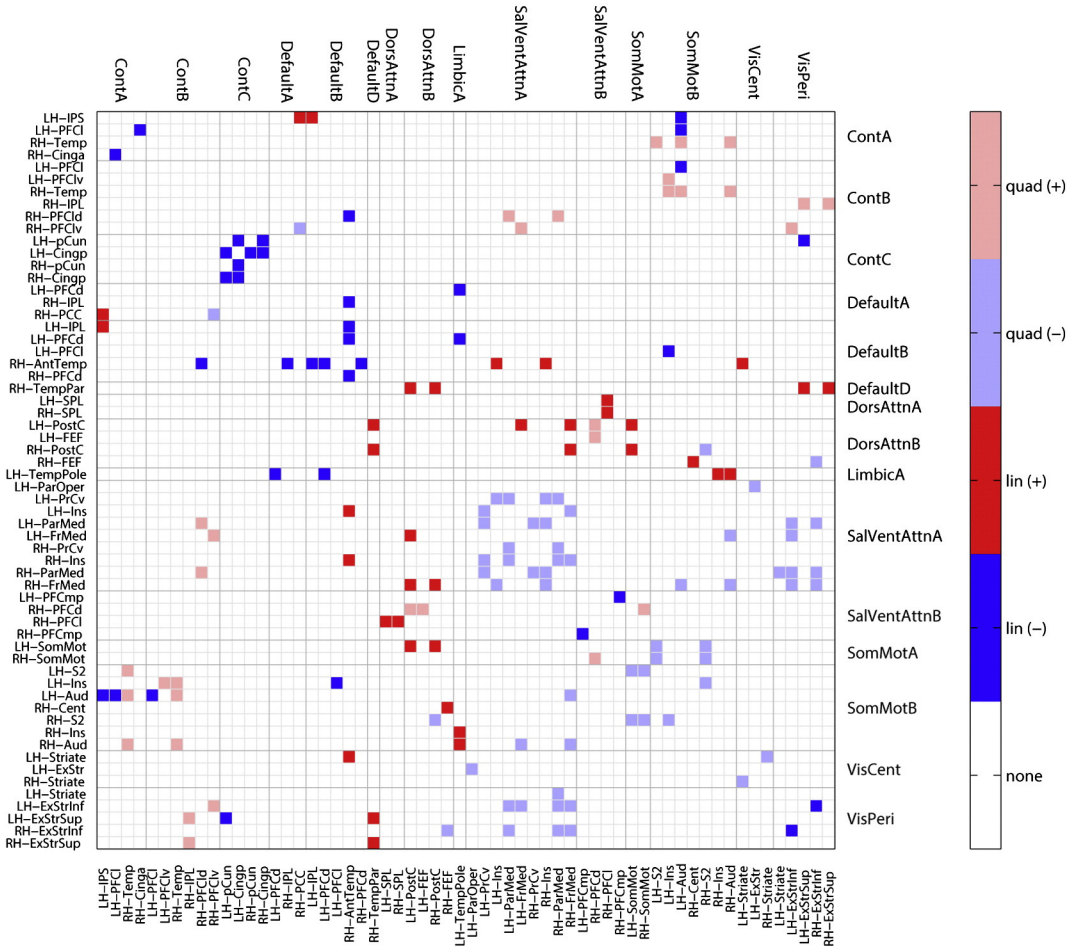

Fig. 4. Statistically significant MLR models ($q < 0.01$, FDR-corrected) fit to individual functional connections. Cell color denotes model order and type: linear increasing (red), linear decreasing (blue), quadratic concave (pink), and quadratic convex (pale blue). See SI Table 1 for MLR model parameters and other details.

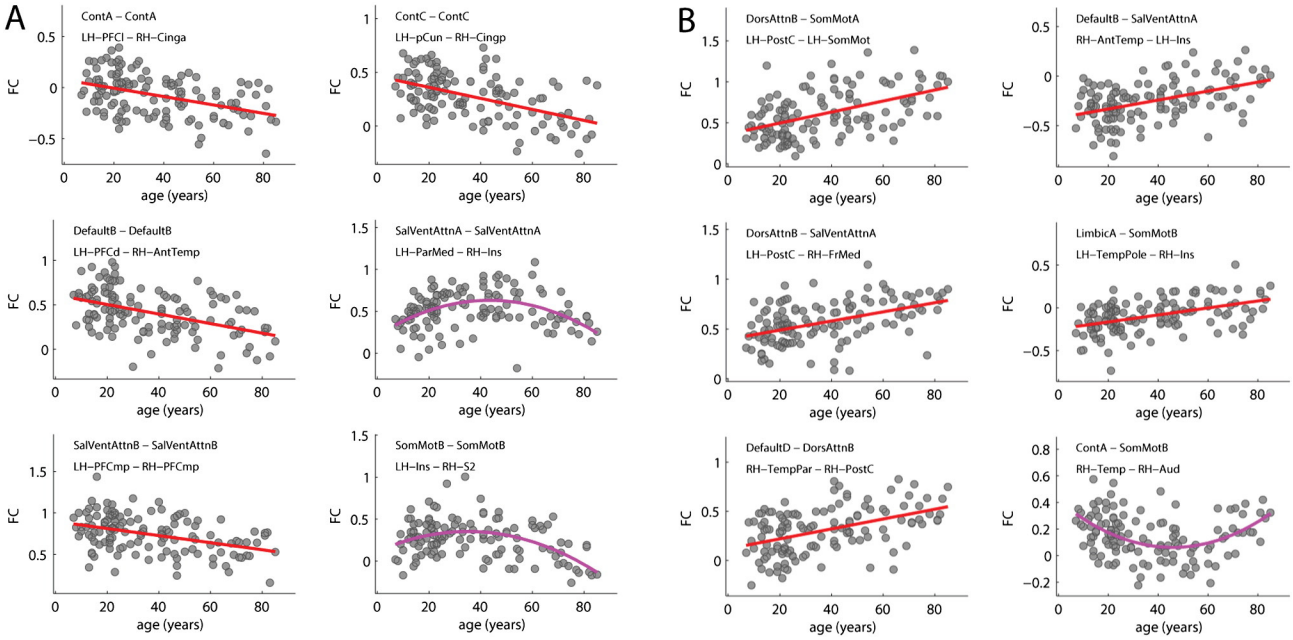

Fig. 5. Representative examples of age-related changes in within-component FC (A) and between-component FC (B). Gray dots indicate empirical estimates of FC while red lines represent the best-fit line derived from the MLR models. All MLR models passed a statistical threshold of $q < 0.01$, FDR-corrected.

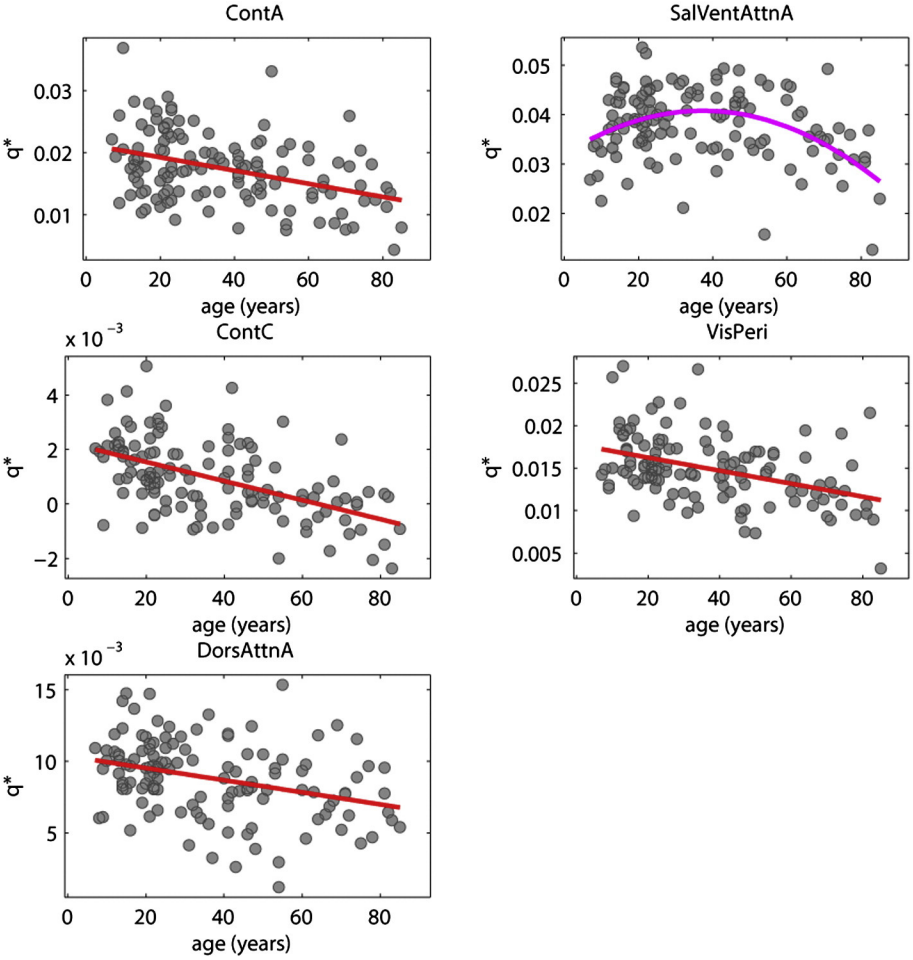

Fig. 6. Statistically significant MLR models ($q < 0.01$, FDR-corrected) fit to individual RSN component modularity, q^*_{RSN}. See SI Table 2 for MLR model parameters and other details.

RSNs modularity decreases with age

The results of the previous section addressed questions about how the magnitude of specific functional connections changed over the course of the entire lifespan. We also assessed system-level change by calculating each RSN component's modularity, q^*_{RSN}, and modeling its change with age. Of the 17 RSN components, five exhibited statistically significant age-related changes ($q < 0.01$, FDR-corrected; corresponding to an uncorrected $p = 1.2 \times 10^{-3}$): ContA, ContC, DorsAttnA, SalVentAttnA, and VisPeri (Fig. 5). Of those five, all but SalVentAttnA were linear, and all predicted a net decrease in modularity over the entire lifespan (Fig. 6). A complete description of all statistically significant models and their parameters can be found in SI Table 2.

Structural changes across the lifespan

In addition to quantifying FC changes over the lifespan, we were also interested in assessing whether SC changed as well. As a coarse measure of change, we first measured the total number of connections, *m*, the total fiber count, *nf*, and the average FA of fibers, *fa*, and modeled their trajectories across the lifespan. Both *m* and *nf* exhibited statistically significant linear decreases with age ($p < 0.01$, uncorrected) (Figs. 7A, B). The variable *fa* exhibited a more complicated trajectory, exhibiting a sharp rise from early childhood into adulthood followed by a protracted decrease (Fig. 7C). This trajectory could not be modeled accurately using either a linear or quadratic model.

Communication capacity decreases in proportion to "hubness"

We next identified a set of hub regions according to a composite score based on their degree (k_i), strength (s_i), nodal efficiency (e_i), and betweenness centrality (b_i). Hubs were consistent across age and levels of γ (SI Fig. 1) and were located bilaterally in extra-striate cortex and in the posterior cingulate, which agree with structural core regions in the posterior-medial cortex reported by Hagmann et al. (2008) and the high-centrality regions reported by Zuo et al. (2012). Other hub regions included the insula, the primary somatomotor cortex, the lateral/ventral prefrontal, and post-central cortices (Fig. 8A).

An important question was whether SC changes across the lifespan would predict increases or decreases in the capacity for communication between brain regions. To address this question, we computed the efficiency of the shortest weighted path connecting every pair of nodes and modeled its trajectory across the lifespan. We found that path efficiency between a large number of nodes decreased with age. Interestingly, statistically significant decreases in path efficiency were not equally distributed, with a small subset of nodes participating in a disproportionate number of statistically significant models ($q < 0.01$, FDR-corrected; corresponding to an uncorrected $p = 2.8 \times 10^{-3}$). Interestingly, the number of statistically significant models that a node participated in was correlated with its "hubness" (Fig. 8B), a relationship that was consistent across the γ values tested in this paper (SI Fig. 2). Because almost all statistically significant models represent decreases in path efficiency, the more statistically significant models a region is involved in, the less efficient that region's connectivity to the rest of the network becomes. This result suggests that a region's "hubness" is a good predictor of whether that region's communication efficiency becomes compromised with age. These findings were robust with respect to alternative edge-weighting schemes such as those that correct edge weights for ROI size (SI Figs. 3 and 4) and were also independent of whether we use more traditional measures to define hubness (i.e. when defining hubness based on node degree, strength, betweenness, or local efficiency, alone) (SI Fig. 5).

Magnitude of age × FC correlation is dependent upon topological distance

The final analysis consisted of assessing whether the numbers of steps separating two nodes in SC was related to the effect of age on FC between those nodes. These results revealed that when nodes are directly connected to one another, their FC is only weakly correlated with age (Fig. 8C). That is, nodes that maintain direct structural connections, on average, also maintain a relatively constant level of FC across the lifespan. As the number of steps increases, however, the correlation between FC and age increases in magnitude. This suggests that with age, FC along multi-step paths becomes stronger, a trend that continues up to a path length of around 4 or 5 steps, partly dependent upon the exact value of γ. This indicates that nodes that are indirectly connected structurally tend to exhibit functional connections that grow stronger over the human lifespan.

Discussion

In this study, we examined changes in functional connectivity and structural connectivity within and between resting-state networks across the human lifespan. Our results indicated that FC within RSNs decreased with age, affecting higher order control and attention networks, visual and somatomotor networks, as well as the default mode network. On the other hand, FC tended to increase between RSNs, especially among components of the dorsal attention network, the saliency/ventral attention networks and the somatomotor network. These results were supported by an additional finding suggesting that the modularity of RSN components comprising control, attentional, limbic, and visual networks decreases with age. Other RSNs, including components of the default mode, also exhibited decreased modularity, but failed to pass a statistical threshold for significance. The density of anatomical connections and the total number of fiber tracts decreased with age, which has the effect of increasing the topological distance and thus decreasing the efficiency of paths between pairs of nodes. Hub regions were affected the most by the decreased number of connections, exhibiting statistically significant decreases in path efficiency with many other regions. Finally, we also observed that the relationship between age and FC depended on path length, a measure derived from SC. For directly connected pairs of nodes, the correlation between age and FC was weakly positive. With greater path length, the magnitude of this correlation progressively increased. Our results suggest

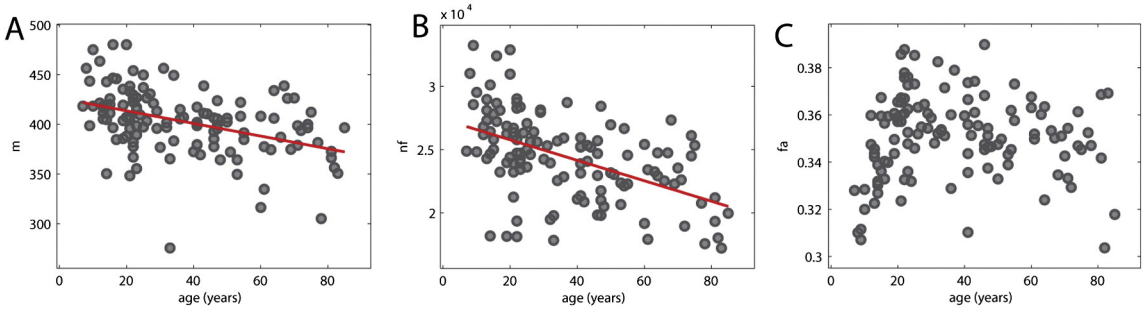

Fig. 7. Change in global SC parameters as a function of age. (A) Number of binary connections, *m*; (B) total fiber count, *nf*; (C) average fractional anisotropy, *fa*.

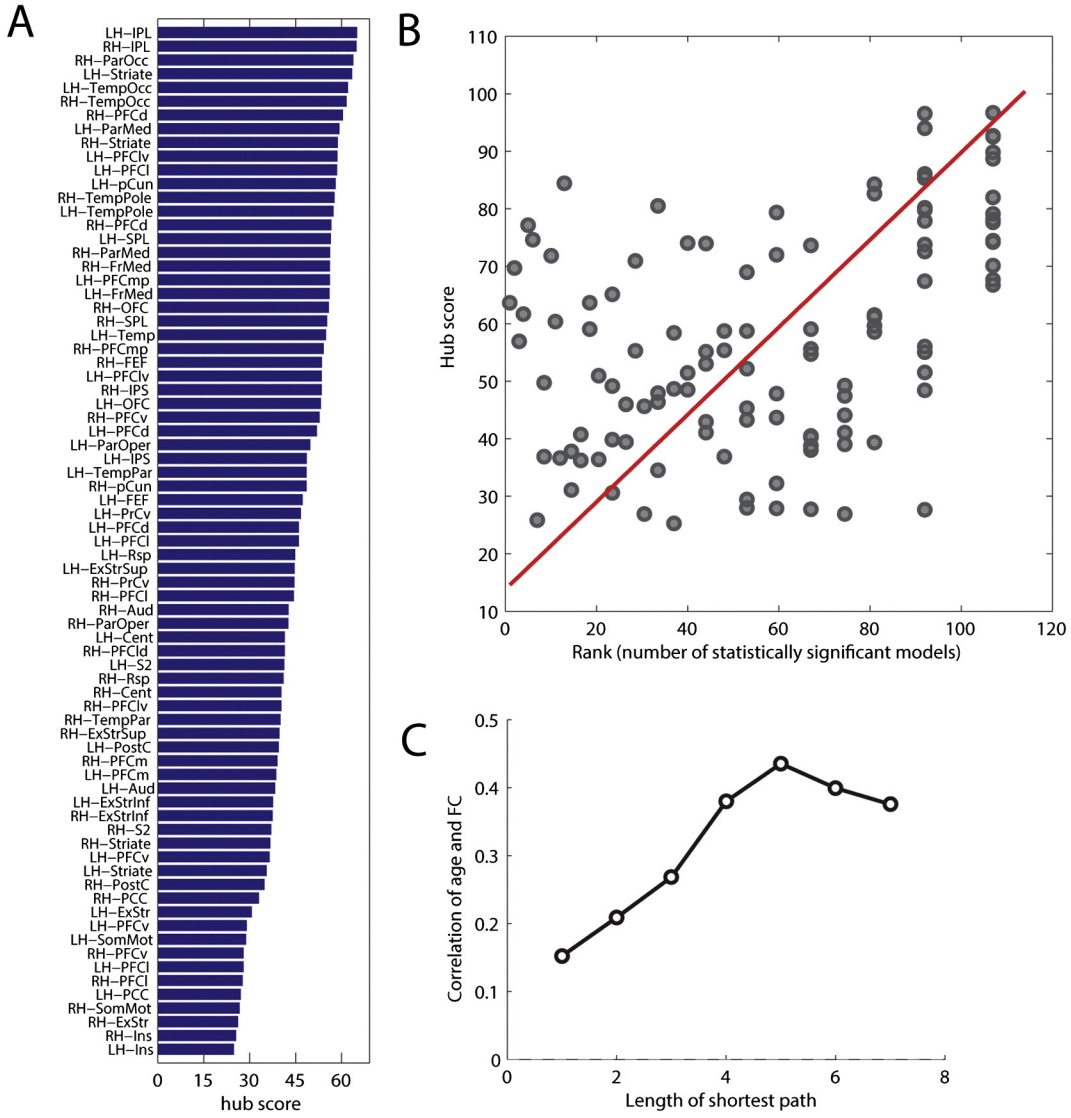

Fig. 8. (A) The average hub scores of the 75 most hub-like regions; (B) a rank-wise scatterplot of hubness as a function of the number of statistically significant models a region participates in; (C) the black line indicates the magnitude of the age by FC correlation of all edges at a given topological distance; the red bars indicate the cumulative percent of all paths less than or equal to a given topological distance. The fraction of all paths with length less than or equal to 7 is 86.6%.

anatomically specific and inter-related patterns of change in FC and SC both within and between RSNs, with a decline in the density of structural connections, particularly at hub nodes, that is associated with a loss of RSN component modularity.

Lifespan changes in functional connectivity

Our first set of results recorded FC changes within and between RSNs. The most consistent observation we made was that FC within RSN components decreased over the lifespan (Fig. 3). FC of regions within ContA, ContC, DefaultB, and VisPeri exhibited a persistent decline over the entire age range considered in this study. SalVentAttnA, SomMotB, and VisCent initially increased their internal FC, but those increases were offset by larger decreases later in life so that the net change in FC was negative (Fig. 4; SI Table 1). These observations are consistent with other studies that have reported age-related decreases in RSN FC, including the default mode (Andrews-Hanna et al., 2007; Geerlings et al., 2014; Tomasi and Volkow, 2012), saliency (Onada et al., 2012), dorsal attention (Andrews-Hanna et al., 2007; Tomasi and Volkow, 2012), control (Geerlings et al., 2014), and visual (Yan et al., 2011) networks. A number of studies reported age-related increases in FC within motor cortices (Meier et al., 2012; Tomasi and Volkow, 2012), which were not observed here. This is likely due to the choice of a conservative statistical threshold; relaxing the critical p-value to $p < 0.05$ (uncorrected) reveals that FC between regions in SomMotA increases with age, corroborating these earlier results.

In addition to FC within RSNs, we also observed age-related changes in FC between different RSN components, most of which involved increased FC, including results that were consistent with earlier findings. For example, Geerlings et al. (2014) reported increased FC between default mode and control networks, as well as visual and control networks, both of which were observed here (ContA increased FC with DefaultA, DefaultB; VisPeri increased FC with ContB). We also reported a number of apparently novel age-related, between-RSN changes in FC: including increased FC between dorsal attention components and components from both motor and saliency/ventral attention networks (DorsAttnB increased FC with SomMotA, SomMotB, SalVentAttnA, SalVentAttnB). Additionally, we observed components of the default mode network that both increased and decreased FC with respect to regions in the control network, as well as increasing FC with the saliency/ventral attention network (DefaultB increased FC with ContA and SalVentAttnA but decreased its FC with respect to ContB and DefaultA).

A number of developmental studies have reported that higher-order cognitive systems (e.g. default mode, control, attentional networks) are not yet mature by early childhood (Fair et al., 2007, 2008, 2009; Jolles et al., 2013; Supekar et al., 2009). These results suggest that over development, we should see increased FC within these networks. In most cases, however, we observe linear decreases within higher-order RSNs (the exception being saliency/ventral attention), possibly due to the fact that the age ranges covering early childhood and adolescence were under-represented in the participant cohort.

The results of the FC analysis can be summarized succinctly by the modularity analysis, revealing modularity changes in ContA, ContC, DorsAttnA, SalVentAttnA, and VisPeri (Fig. 6). The modularity measurement can fluctuate as a consequence of decreased internal or increased external FC. ContA, ContC, and VsiPeri all exhibit decreased internal FC, which likely causes their modularity to decrease. The decrease in modularity of DorsAttnA, on the other hand, is due primarily to its increased connectivity to other RSNs, for example, SalVentAttnB. The quadratic trajectory of SalVentAttnA is likely due to a combination of both effects; functional connections within SalVentAttnA exhibit similar convex trajectories across the lifespan, while SalVentAttnA also becomes more strongly coupled to DorsAttnB, DefaultB, and ContB, which increases its external FC and drives its modularity downward. Interestingly, no default mode network components exhibited statistically significant modularity decreases despite the fact that many studies have reported decreases in their internal FC with aging (Andrews-Hanna et al., 2007; Bluhm et al., 2008; Tomasi and Volkow, 2012). This can be explained by the choice of a conservative statistical threshold; with an uncorrected threshold of $p < 0.05$, DefaultA, DefaultC, and DefaultD all exhibit statistically significant decreases in modularity (SI Table 2).

The cross-sectional nature of this study allowed us to model age-related change in FC and SC as continuous variables, which revealed that certain functional connections were best described by quadratic trajectories. In general, these involved a small subset of RSN components, most notably SalVentAttnA, VisPeri, ContA/B, and SomMotA/B. These connections could then be clustered, with SalVentAttnA and VisPeri in one cluster and ContA/B and SomMotA/B in the other. This division is notable, and is suggestive of systems associated with visual attention and motor planning that develop, mature, and age in unison. Both clusters also involve the insular cortex, which was not only identified as a structural hub region in this study, but has also been described as a key functional hub (Craig, 2009). The insular cortex has been implicated in conditions related to awareness and self-reference (Klein et al., 2007), and maintains strong functional connections to both cognitive control systems and the motor cortex (Menon and Udding, 2010).

Lifespan changes in structural connectivity

In terms of SC, we observed a linear decrease in the total number of streamlines, *nf* (Fig. 7B), which has also been reported elsewhere (Lim et al., 2013). Additionally, average fractional anisotropy, *fa*, reflects the integrity of white-matter fiber tracts and exhibited a steep rise from childhood to early adulthood before beginning a protracted decrease across the remainder of the lifespan (Fig. 7C). This curve is consistent with typical FA maturational trajectories and (Barnea-Goraly et al., 2005; Kochunov et al., 2011; Sullivan and Pfefferbaum, 2006).

Topologically, the most prominent age-related change was a linear decrease in the number of binary connections, *m* (Fig. 7A), an effect that has been previously reported elsewhere (Gong et al., 2009; Lim et al., 2013). The decrease in connection density and average FA with aging largely agrees with the "disconnection" hypothesis, wherein cognitive decline during healthy aging is attributed to compromised white-matter connectivity (O'Sullivan et al., 2001).

Despite the ongoing changes in network sparsity, we observed a consistent set of highly connected, highly central hub regions. The regions comprising the hubs actually changed very little over the course of the lifespan, which is consistent with findings of a consistent set of hub regions in preterm infants (Yap et al., 2011), during development (Chen et al., 2013; Hagmann et al., 2010), adulthood (Hagmann et al., 2008), and throughout aging (Gong et al., 2009). Despite the relative constancy of hub regions, the decrease in number of connections effectively sparsified the network, leading to decreased path efficiency with age. Hence, later in life many pairs of nodes were anatomically linked by less efficient paths. We examined this effect in detail and determined that a small subset of nodes exhibited decreased path efficiency with respect to a large number of other nodes. Overall, hub regions seemed to be more susceptible to decreases in path efficiency than non-hubs (Fig. 8B). This finding does not necessarily indicate that hubs are selectively becoming more disconnected or that their connectivity is altered preferentially. A possible alternative explanation rests on the fact that hub regions form more connections than non-hub regions; if one selects a connection at random, it is more likely that the connection interfaces with a hub region than a non-hub region.

Implications for lifespan changes in communication patterns

There is mounting evidence that SC and FC are closely related to one another, with SC thought to exert a causal influence over FC patterns (Hermundstad et al., 2013; Honey et al., 2009; O'Reilly et al., 2013). While the precise causal role is not fully understood, it has been suggested that SC shapes FC by constraining inter-areal communication processes (Deco et al., 2010; Honey et al., 2009). Indeed, models that incorporate SC have been able to generate synthetic FC patterns that resemble those obtained through empirical brain recordings (Goñi et al., 2014; Haimovici et al., 2013; Honey et al., 2007, 2009).

Given that SC topology influences FC, it was important to quantify the effects of age-related changes in SC on FC. In this study, we observed decreases in overall SC across the lifespan, which led to decreased path efficiency among regions. Decreased path efficiency has implications for how these regions communicate with one another and the extent to which they become functionally connected. Less efficient paths tend to be associated with a decreased likelihood of signal transmission and hence should support weaker functional connectivity. The observed progressive decline in path efficiency with age implies that communication between nodes which early in life occurred via more direct connections or efficient paths requires multi-step, less efficient paths later in life. If the way SC shapes FC remains unchanged, then age-related decreases in path efficiency should lead to a progressive weakening of FC.

However, our analysis indicates that communication along more direct paths shows a different age-related pattern than communication along more indirect paths. The FC of directly connected nodes changes very little, on average, over the entire lifespan. However, as the length of the shortest weighted path connecting nodes increases (with a majority of them connecting nodes that belong to different RSNs), we observed a strengthening of the age-related increase in FC in the form of a stronger linear correlation (Fig. 8C). These findings suggest that early in life inter-areal communication is facilitated predominantly by short, efficient paths but that later in life, multi-step paths become increasingly efficacious in supporting high functional connectivity. A corollary of the observed "thinning" of structural connectivity with age is that there are also fewer edges that are available for transmitting neural signals, which means that the number of shortest paths traversing a given edge is also expected to increase.

An alternative interpretation of these results is based on time-varying FC (Allen et al., 2014; Hutchinson et al., 2013). Our interpretation of age-related changes in FC is that changes in FC magnitude reflect increased or decreased coupling between brain regions. This view is dependent upon the static characterization of FC, where each pair of regions is assigned a single scalar (correlation) value representing the average FC over the entire scan session. On the other hand, the time-varying approach divides the BOLD time series into overlapping windows and estimates FC for each window independently, yielding for every connection a series of correlation values. In this light, changes

in average FC can be accounted for not by changes in coupling strength, but by dynamic changes in the level of FC over the course of a scan session; functional connections that become more variable with age may converge towards lower overall FC strength while connections that become less variable may show the opposite effect. Time-varying FC across the lifespan was not investigated in this report, but is a topic worthy of future investigation.

How age-related changes in functional and structural connectivity within and between RSNs relate to changes in behavior and cognition is another important question for future research. The observed age-related decreases in cohesiveness of RSNs could potentially underlie the increasingly correlated task performance across different domains observed with aging (Li et al., 2001). However, such decreases in RSN coherence could reflect compensatory increases in cortical recruitment associated with relatively preserved performance (Buckner, 2004) or cortical de-differentiation linked with cognitive and behavioral decline (e.g. Park et al., 2010). Future longitudinal research incorporating neuropsychological measures will be able to evaluate these possibilities and their relative specificity (e.g. whether decreased coherence of attention networks specifically is uniquely positively or negatively correlated with well-documented age-related deficits in attentional mechanisms; Li et al., 2001) and the extent to which different aspects of the RSN connectivity changes reported here are linked more directly with changes in age or changes in performance (as in Dosenbach et al., 2010). Finally, the current findings are suggestive of changes to structural integrity (including myelin deterioration and vascular insult; Buckner, 2004; Tomasi and Volkow, 2012) leading to increased reliance on polysynaptic structural paths and thus increased functional coordination over them (see also Hawellek et al., 2011), but this cross-sectional design cannot disambiguate the direction of that relationship. Active enrichment (cognitive, social, and physical) is increasingly shown to preserve and even increase cognitive performance in aging (Hertzog et al., 2009). Future longitudinal research providing such enrichment both before and after "thinning" of white matter is observed will shed light on the mechanisms underlying this changing relationship between functional and structural connectivity as well as provide critical insights into the general preservation of function in aging.

Limitations of current study

There are a number of limitations to this study, related to MR preprocessing, node definition and parcellation, modeling approach, as well as participant cohort and age range.

The first set of limitations concerns various fMRI and DTI/tractography processing steps. Regarding fMRI, FC between nodes was estimated after regressing out the global BOLD signal. While this is a contentious step because it can induce negative correlations, the interpretation of which is unclear (Chai et al., 2012; Murphy et al., 2009), it has also been shown that it can effectively reduce non-neural noise (Power et al., 2014). A potential confound in developmental fMRI studies is head movement. We addressed this confound in two different ways. First, in our pre-processing of the fMRI data, we used the Friston-24 regression model with an additional motion parameter, which contributes to reduce motion artifacts (Yan et al., 2013). Second, in our MLR analysis, we included mean frame-wise displacement as a nuisance parameter, allowing it to compete with age terms to explain variance in FC and other measures (Cao et al., 2014). Regarding DTI/tractography, the present study faces several standard challenges, including detection of long-distance connections, resolving crossing fibers, as well as variations in FA across age. Overall, SC networks reconstructed in the present study exhibit attributes that are consistent with a previous work (Mwangi et al., 2013), including age-related changes in FA (Barnea-Goraly et al., 2005; Kochunov et al., 2011; Sullivan and Pfefferbaum, 2006) and network density (Gong et al., 2009; Lim et al., 2013), as well as hub distributions (Chen et al., 2013; Gong et al., 2009; Hagmann et al., 2008; Yap et al., 2011).

Another set of limitations concerns the important step of node definition. Since we were interested in FC/SC relationships within and between RSNs, we used a parcellation that was based on a standard partition of the cortex into a canonical set of functional systems or RSNs (Yeo et al., 2011), which was in line with approaches taken in previous work (Baker et al., 2013; Geerlings et al., 2014). This parcellation was created based on a cohort of younger participants (~21 years old), which raises the question whether it is equally appropriate for the youngest and oldest subjects in this study. In a recent paper by Cao et al. (2014) that used the same dataset as this study, the authors reported that most (but not all) of their results were independent of parcellation choice. In particular, the authors used three parcellations: the Yeo parcellation used here and two other parcellations that divided the cortex into 160 and 1024 regions. Rich-club coefficients, global efficiency, modularity, and connectivity strength all demonstrated consistent age-related changes across the three parcellations. While the debate over the appropriate regional division of the brain is ongoing, future work on data-driven parcellation will allow more sensitive assessments of age-related changes in both FC and SC.

Another possible limitation was the choice to model lifespan trajectories of variables of interest as either linear or quadratic curves. While MLR models of this type have been widely used in the study of age-related changes in brain networks, they have some inherent limitations (Cao et al., 2014; Zuo et al., 2010). One of the main limitations is that first and second order polynomial models may not capture higher-order behavior — i.e. variables that exhibit complicated trajectories over the lifespan might be poorly modeled by linear and quadratic curves. In future work it would be useful to explore other modeling options, such as non-parametric locally weighted regression (Cleveland and Devlin, 1988) or sliding boxcar techniques, which have been used before to model age-related changes in functional brain networks (Fair et al., 2009). We did not explore such options in this paper, as we were interested in having closed form, analytic expressions for variables of interest as a function of age, which are given by the beta coefficients of MLR models but not by the other methods mentioned here. Other options for analyzing these data include multivariate measures, such as partial least squares, which could be useful for identifying patterns of connections (either functional or structural) that collectively covary with age (McIntosh and Mišić, 2013).

A final set of limitations concerns the limited age range covered by the participant cohort which did not cover the early postnatal period (ages 0–7 years) and did not cover all age groups evenly. We would expect that the inclusion of infants and young children would likely impact some of the observed linear or non-linear trends in FC and/or SC as the early years are known to be a period of rapid change in all connectivity-related measures.

All of these limitations could be addressed in future work, as more sensitive data acquisition techniques, new pre-processing approaches, data-driven parcellations and extended participant samples become available.

Conclusions

In conclusion, this study represents a multi-modal analysis of brain functional and structural systems and the changes they undergo over the course of late development, adulthood, and aging. Our analyses suggest that RSNs corresponding to both cognitive and sensorimotor functions undergo significant age-related refinement, in general becoming less functionally cohesive with age. We also demonstrate that the brain's white matter integrity, number of fiber tracts, and network sparsity all follow characteristic trajectories. As a consequence of these global changes, the efficiency with which gray matter regions were connected to one another decreased, which may be indicative of an impaired capacity for inter-areal communication. Finally, we observed that the relationship of functional and structural connectivity

changed over the lifespan, so that with age, stronger functional connections are mediated by less efficient, multi-step anatomical paths.

Supplementary data to this article can be found online at http://dx.doi.org/10.1016/j.neuroimage.2014.07.067.

Acknowledgments

RFB was supported by the National Science Foundation/Integrative Graduate Education and Research Traineeship Training Program in the Dynamics of Brain–Body–Environment Systems at Indiana University (#0903495). LB was supported by a National Science Foundation Graduate Research Fellowship. JG and OS were supported by the JS McDonnell Foundation (#22002082). XNZ acknowledges funding support from the Hundred Talents Program, the Key Research Program (KSZD-EW-TZ-002) of the Chinese Academy of Sciences and the National Natural Science Foundation of China (81171409, 81220108014).

Conflict of interest

The authors declare no conflicting interests.

References

Achard, S., Bullmore, E.T., 2006. Efficiency and cost of economical brain functional networks. PLoS Comput. Biol. 3 (2), e17.
Achard, S., Salvador, R., Whitcher, B., Suckling, J., Bullmore, E.T., 2006. A resilient, low-frequency small-world human brain functional network with highly connected association cortical hubs. J. Neurosci. 26 (1), 63–72.
Allen, E.A., Damaraju, E., Plis, S.M., Erhardt, E.B., Eichele, T., Calhoun, V.D., 2014. Tracking whole-brain connectivity dynamics in the resting state. Cereb. Cortex 24 (3), 663–676.
Andersson, J.L.R., Skare, S., 2002. A model-based method for retrospective correction of geometric distortions in diffusion-weighed EPI. Neuroimage 16 (1), 177–199.
Andrews-Hanna, J.R., Snyder, A.Z., Vincent, J.L., Lustig, C., Head, D., Raichle, M.E., Buckner, R. L., 2007. Disruption of large-scale brain systems in advanced aging. Neuron 56 (5), 924–935.
Baker, J.T., Holmes, A.J., Masters, G.A., Yeo, B.T.T., Krienen, F., Buckner, R.L., Ongur, D., 2013. Disruption of cortical association networks in schizophrenia and psychotic bipolar order. JAMA Psychiatry 71 (2), 109–118.
Barnea-Goraly, N., Menon, V., Eckert, M., Tamm, L., Bammer, R., Karchemskiy, A., Dant, C.C., Reiss, A.L., 2005. White matter development during childhood and adolescence: a cross-sectional diffusion tensor imaging study. Cereb. Cortex 15 (12), 1848–1854.
Bassett, D.S., Greenfield, D.L., Meyer-Lindenberg, A., Weinberger, D.R., Moore, S.W., Bullmore, E.T., 2010. Efficient physical embedding of topologically complex information processing networks in brains and computer circuits. PLoS Comput. Biol. 6 (4), e1000748.
Beckmann, C.F., DeLuca, M., Devlin, J.T., Smith, S.M., 2005. Investigations into resting-state connectivity using independent component analysis. Philos. Trans. R. Soc. B 360, 1001–1013.
Bellec, P., Rosa-Neto-, P., Lyttelton, O.C., Benali, H., Evans, A.C., 2010. Multi-level bootstrap analysis of stable clusters in resting-state fMRI. Neuroimage 51 (3), 1126–1139.
Benjamini, Y., Hochberg, Y., 1995. Controlling the false discovery rate: a practical and powerful approach to multiple testing. J. R. Stat. Soc. 57 (1), 289–300.
Betzel, R.F., Griffa, A., Avena-Koenigsberger, A., Goñi, J., Hagmann, P., Thiran, J.P., Sporns, O., 2013. Multi-scale community organization of the human structural connectome and its relationship with resting-state functional connectivity. Netw. Sci. 1 (3), 353–373.
Bluhm, R.L., Osuch, E.A., Lanius, R.A., Boksman, K., Neufeld, R.W., Theberge, J., Williamson, P., 2008. Default mode network connectivity: effects of age, sex, and analytic approach. Neuroreport 19 (8), 887–891.
Buckner, R.L., 2004. Memory and executive function in aging and AD: multiple factors that cause decline and reserve factors that compensate. Neuron 44 (1), 195–208.
Buckner, R.L., Krienen, F.M., Yeo, B.T., 2013. Opportunities and limitations of intrinsic functional connectivity MRI. Nat. Neurosci. 16 (7), 832–837.
Bullmore, E.T., Sporns, O., 2009. Complex brain networks: graph theoretical analysis of structural and functional systems. Nat. Rev. Neurosci. 10 (3), 186–198.
Bullmore, E.T., Sporns, O., 2012. The economy of brain network organization. Nat. Rev. Neurosci. 13 (5), 336–349.
Cao, M., Wang, J.H., Dai, Z.J., Cao, X.Y., L.L.J., Fan, F.M., Song, X.W., Xia, M.R., Shu, N., Dong, Q., Milham, M.P., Castellanos, F.X., Zuo, X.N., He, Y., 2014. Topological organization of the human brain functional connectome across the lifespan. Dev. Cogn. Neurosci. 7, 76–93.
Chai, X.J., Castanon, A.N., Ongur, D., Whitfield-Gabrieli, S., 2012. Anticorrelations in resting state networks without global signal regression. Neuroimage 59 (2), 1420–1428.
Chang, L.C., Jones, D.K., Pierpaoli, C., 2005. RESTORE: robust estimation of tensors by outlier rejection. Magn. Reson. Med. 53 (5), 1088–1095.
Chen, Z., Liu, M., Gross, D.W., Beaulieu, C., 2013. Graph theoretical analysis of developmental patterns of the white matter network. Front. Hum. Neurosci. 7.
Cleveland, W.S., Devlin, S.J., 1988. Locally-weighted regression: an approach to regression analysis by local fitting. J. Am. Stat. Assoc. 35 (1), 596–610.
Craig, A.D., 2009. How do you feel — now? The anterior insula and human awareness. Nat. Rev. Neurosci. 10 (1), 59–70.
Crossley, N.A., Mechelli, A., Vertes, P.E., Winton-Brown, T.T., Patel, A.X., Ginestet, C.E., McGuire, P., Bullmore, E.T., 2013. Cognitive relevance of the community structure of the human brain functional coactivation network. Proc. Natl. Acad. Sci. U. S. A. 110 (28), 11583–11588.
Deco, G., Jirsa, V.K., McIntosh, A.R., 2010. Emerging concepts for the dynamical organization of resting-state activity in the brain. Nat. Rev. Neurosci. 12 (1), 43–56.
Dijkstra, E.W., 1959. A note on two problems in connexion with graphs. Numer. Math. 1 (1), 269–271.
Dosenbach, N.U., Nardos, B., Cohen, A.L., Fair, D.A., Power, J.D., et al., 2010. Prediction of individual brain maturity using fMRI. Science 329 (5997), 1358–1361.
Fair, D.A., Dosenbach, N.U., Church, J.A., Cohen, A.L., Brahmbhatt, S., Miezin, F.M., Barch, D.M., Raichle, M.E., Petersen, S.E., Schlaggar, B.L., 2007. Development of distinct control networks through segregation and integration. Proc. Natl. Acad. Sci. U. S. A. 104 (33), 13507–13512.
Fair, D.A., Cohen, A.L., Dosenbach, N.U., Church, J.A., Miezin, F.M., Barch, D.M., Raichle, M.E., Petersen, S.E., Schlaggar, B.L., 2008. The maturing architecture of the brain's default network. Proc. Natl. Acad. Sci. U. S. A. 105 (10), 4028–4032.
Fair, D.A., Cohen, A.L., Power, J.D., Dosenbach, N.U.F., Church, J.A., Miezin, F.M., Schlaggar, B.L., Petersen, S.E., 2009. Functional brain networks develop from a "local to distributed" organization. PLoS Comput. Biol. 5 (5), e1000381.
Ferreira, L.K., Busatto, G.F., 2013. Resting-state functional connectivity in normal brain aging. Neurosci. Biobehav. Rev. 37 (3), 384–400.
Friston, K.J., Williams, S., Howard, R., Frackowiak, R.S., Turner, R., 1996. Movement-related effects in fMRI time-series. Magn. Reson. Med. 35, 346–355.
Geerlings, L., Renken, R.J., Saliasi, E., Maurits, N.M., Lorist, M.M., 2014. A brain-wide study of age-related changes in functional connectivity. Cereb. Cortex http://dx.doi.org/10.1093/cercor/bhu012.
Gong, G., He, Y., Concha, L., Lebel, C., Gross, D.W., Evans, A.C., Beulieu, C., 2009. Mapping anatomical connectivity patterns of human cerebral cortex using in vivo diffusion tensor imaging tractography. Cereb. Cortex 19 (3), 524–536.
Goñi, J., van den Heuvel, M.P., Avena-Koenigsberger, A., de Mendizábal, N.V., Betzel, R.F., Griffa, A., Hagmann, P., Corominas-Murtra, B., Thiran, J.P., Sporns, O., 2014. Resting-brain functional connectivity predicted by analytic measures of network communication. Proc. Natl. Acad. Sci. 111 (2), 833–838.
Hagmann, P., Cammoun, L., Gigandet, X., Meuli, R., Honey, C.J., Wedeen, V.J., Sporns, O., 2008. Mapping the structural core of human cerebral cortex. PLoS Biol. 6 (7), e159.
Hagmann, P., Sporns, O., Madan, N., Cammoun, L., Pienaar, R., Wedeen, V.J., Meuli, R., Thiran, J.P., Grant, P.E., 2010. White matter maturation reshapes structural connectivity in the late developing human brain. Proc. Natl. Acad. Sci. 107 (44), 19067–19072.
Haimovici, A., Tagliazucchi, E., Balenzuela, P., Chialvo, D.R., 2013. Brain organization into resting state networks emerges at criticality on a model of the human connectome. Phys. Rev. Lett. 110 (17), 178101.
Hawellek, D.J., Hipp, J.F., Lewis, C.M., Corbetta, M., Engel, A.K., 2011. Increased functional connectivity indicates the severity of cognitive impairment in multiple sclerosis. Proc. Natl. Acad. Sci. 108 (47), 19066–19071.
Hermundstad, A.M., Bassett, D.S., Brown, K.S., Aminoff, E.M., Clewett, D., Freeman, S., Frithsen, A., Johnson, A., Tipper, C.M., Miller, M.B., Grafton, S.T., Carlson, J.M., 2013. Structural foundations of resting-state and task-based functional connectivity in the human brain. Proc. Natl. Acad. Sci. 110 (5), 6169–6174.
Hertzog, C., Kramer, A.F., Wilson, R.S., Lindenberger, U., 2009. Enrichment effects on adult cognitive development: can the functional capacity of older adults be preserved and enhanced? Psychol. Sci. Public Interest 9 (1), 1–65.
Honey, C.J., Kotter, R., Breakspear, M., Sporns, O., 2007. Network structure of cerebral cortex shapes functional connectivity on multiple time scales. Proc. Natl. Acad. Sci. 104 (24), 10240–10245.
Honey, C.J., Sporns, O., Cammoun, L., Gigandet, X., Thiran, J.P., Meuli, R., Hagmann, P., 2009. Predicting human resting-state functional connectivity from structural connectivity. Proc. Natl. Acad. Sci. 106 (6), 2035–2040.
Hutchinson, R.M., Wornelsdorf, T., Allen, E.A., Bandettini, P.A., Calhoun, V.D., Corbetta, M., Della Penna, S., Duyn, J.H., Glover, G.H., Gonzalez-Castillo, J., Handwerker, D.A., Keilholz, S., Kiviniemi, V., Leopold, D.A., de Pasquale, F., Sporns, O., Walter, M., Chang, C., 2013. Dynamic functional connectivity: promise, issues, and interpretations. Neuroimage 80, 360–378.
Jiang, L., Xu, T., Ye He, X.H., Hou, J. Wang, Cao, X.Y., Wei, G.X., Yang, Z., He, Y., Zuo, X.N., 2014. Toward neurobiological characterization of functional homogeneity in the human cortex: regional variation, morphological association and functional covariance network organization. Brain Struct. Funct. 1–23.
Jolles, D.D., van Buchem, M.A., Crone, E.A., Rombouts, S.A., 2013. Functional brain connectivity at rest changes after working memory training. Hum. Brain Mapp. 34 (2), 396–406.
Kelly, A.M.C., Di Martino, A., Uddin, L.Q., Shehzad, Z., Gee, D.G., Reiss, P.T., Margulies, D.S., Castellanos, F.X., Milham, M.P., 2009. Development of anterior cingulate functional connectivity from late childhood to early adulthood. Cereb. Cortex 19 (3), 640–657.
Klein, T.A., Endrass, T., Kathmann, N., Neumann, J., Von Cramon, D.Y., Ullsperger, M., 2007. Neural correlates of error awareness. Neuroimage 34 (4), 1774–1781.
Kochunov, P., Glahn, D.C., Lancaster, J., Thompson, P.M., Kochunov, V., Rogers, B., Fox, P., Blangero, J., Williamson, D.E., 2011. Fractional anisotropy of cerebral white matter and thickness of cortical gray matter across the lifespan. Neuroimage 58 (1), 41–49.
Latora, V., Marchiori, M., 2001. Efficient behavior of small-world networks. Phys. Rev. Lett. 87 (19), 198701.
Lewis, C.M., Baldassarre, A., Committeri, G., Romani, G.L., Corbetta, M., 2009. Learning sculpts the spontaneous activity of the resting human brain. Proc. Natl. Acad. Sci. 106 (41), 17558–17563.

Li, S.C., Lindenberger, U., Sikström, S., 2001. Aging cognition: from neuromodulation to representation. Trends Cogn. Sci. 5 (11), 479–486.
Lim, S., Han, C.E., Uhlhaas, P.J., Kaiser, M., 2013. Preferential detachment during human brain development: age- and sex-specific structural connectivity in diffusion tensor imaging (DTI) data. Cereb. Cortex http://dx.doi.org/10.1093/cercor/bht333.
Lohse, C., Bassett, D.S., Lim, K.O., Carlson, J.M., 2013. Resolving structure in human brain organization: identifying mesoscale organization in weighted network representations, (arXiv, preprint arXiv:1312.6070).
Ma, L., Narayana, S., Robin, D.A., Fox, P.T., Xiong, J., 2011. Changes occur in resting state network of motor system during 4 weeks of motor skill learning. Neuroimage 58 (1), 226–233.
McIntosh, A.R., Mišić, B., 2013. Multivariate statistical analysis for neuroimaging data. Annu. Rev. Psychol. 64, 499–525.
Meier, T.B., Desphande, A.S., Vergun, S., Nair, V.A., Song, J., Biswal, B.B., Meyerand, M.E., Birn, R.M., Prabhakaran, V., 2012. Support vector machine classification and characterization of age-related reorganization of functional brain networks. Neuroimage 60 (1), 601–613.
Menon, V., Udding, L., 2010. Saliency, switching, attention and control: a network model of insula function. Brain Struct. Funct. 214 (5–6), 655–667.
Meunier, D., Lambiotte, R., Fornito, A., Ersche, K.D., Bullmore, E.T., 2009. Hierarchical modularity in human brain functional networks. Front. Neuroinf. 3 (37), 1–12.
Meunier, D., Lambiotte, R., Bullmore, E.T., 2010. Modular and hierarchically modular organization of brain networks. Front. Neurosci. 4, 200.
Mori, S., van Zilj, P.C., 2002. Fiber tracking: principles and strategies — a technical review. NMR Biomed. 15 (7–8), 468–480.
Mori, S., Crain, B.J., Chacko, V.P., van Zilj, P.C., 1999. Three-dimensional tracking of axonal projections in the brain by magnetic resonance imaging. Ann. Neurol. 45 (2), 265–269.
Murphy, K., Birn, R.M., Handwerker, D.A., Jones, T.B., Bandettini, P.A., 2009. The impact of global signal regression on resting state correlations: are anti-correlated networks introduced? Neuroimage 44 (3), 893–905.
Mwangi, B., Hasan, K.M., Soares, J.C., 2013. Prediction of individual subject's age across the human lifespan using diffusion tensor imaging: a machine learning approach. Neuroimage 75 (15), 58–67.
Newman, M.E.J., 2006. Modularity and community structure in network. Proc. Natl. Acad. Sci. 103 (23), 8577–8582.
Nooner, K.B., Colcombe, S.L., Tobe, R.H., Mennes, M., Benedict, M.M., Moreno, A.L., Panek, L.J., Brown, S., Zavitz, S.T., Li, Q., Sikka, S., Gutman, D., Bangaru, S., Schlachter, R.T., Kamiel, S. M., Anwar, A.R., Hinz, C.M., Kaplan, M.S., Rachlin, A.B., Adelsberg, S., Cheung, B., Khanuja, R., Yan, C., Craddock, C.C., Calhoun, V., Courtney, W., King, M., Wood, D., Cox, C.L., Kelly, A.M.C., Di Martino, A., Petkova, E., Reiss, P.T., Duan, N., Thomsen, D., Biswal, H., Coffey, B., Hoptman, M.J., Javitt, D.C., Pomara, N., Sidtis, J.S., Koplewicz, H.S., Castellanos, F.X., Leventahl, B.L., Milham, M.P., 2012. The NKI-Rockland sample: a model for accelerating the pace of discover science in psychiatry. Front. Neurosci. 6, 152.
O'Reilly, J.X., Croxson, P.L., Jbabdi, S., Sallet, J., Noonan, M.P., Mars, R.B., Browning, P.G.F., Wilson, C.R.E., Mitchell, A.S., Miller, K.L., Rushworth, M.F.S., Baxter, M.G., 2013. Causal effect off disconnection lesions on interhemispheric functional connectivity in rhesus monkeys. Proc. Natl. Acad. Sci. 110 (34), 13982–13987.
O'Sullivan, M.R.C.P., Jones, D.K., Summers, P.E., Morris, R.G., Williams, S.C.R., Markus, H.S., 2001. Evidence for cortical "disconnections" as a mechanism of age-related cognitive decline. Neurology 57 (4), 632–638.
Onada, K., Ishihara, M., Yamaguchi, S., 2012. Decreased functional connectivity by aging is associated with cognitive decline. J. Cogn. Neurosci. 24 (11), 2186–2198.
Park, J., Carp, J., Hebrank, A., Park, D.C., Polk, T.A., 2010. Neural specificity predicts fluid processing ability in older adults. J. Neurosci. 30 (27), 9253–9259.
Power, J.D., Cohen, A.L., Nelson, S.M., Wig, G.S., Barnes, K.A., Church, J.A., Vogel, A.C., Laumann, T.O., Miezin, F.M., Schlaggar, B.L., Petersen, S.E., 2011. Functional network organization of the human brain. Neuron 72 (4), 665–678.
Power, J.D., Barnes, K.A., Snyder, A.Z., Schlaggar, B.L., Petersen, S.E., 2012. Spurious but systematic correlations in functional connectivity MRI networks arise from subject motion. Neuroimage 59 (3), 2142–2154.
Power, J.D., Mitra, A., Laumann, T.O., Snyder, A.Z., Schlaggar, B.L., Petersen, S.E., 2014. Methods to detect, characterize, and remove motion artifact in resting state fMRI. Neuroimage 84, 320–341.
Rubinov, M., Sporns, O., 2010. Complex network measures of brain connectivity: uses and interpretations. Neuroimage 52 (3), 1059–1069.
Rubinov, M., Sporns, O., 2011. Weight-conserving characterization of complex function brain networks. Neuroimage 56 (4), 2068–2079.
Schwarz, A.J., McGonigle, J., 2011. Negative edges and soft thresholding in complex network analysis of functional connectivity data. Neuroimage 55 (3), 1132–1146.
Smith, S.M., Fox, P.T., Miller, K.L., Glahn, D.C., Fox, P.M., Mackay, C.E., Filippini, N., Watkins, K. E., Toro, R., Laird, A.R., Beckmann, C.F., 2009. Correspondence of the brain's functional architecture during activation and rest. Proc. Natl. Acad. Sci. U. S. A. 106 (31), 13040–13045.
Sporns, O., 2014. Contributions and challenges for network models in cognitive neuroscience. Nat. Rev. Neurosci. 17 (4), 1–9. http://dx.doi.org/10.1038/nn.3690.
Sullivan, E.V., Pfefferbaum, A., 2006. Diffusion tensor imaging and aging. Neurosci. Biobehav. Rev. 30, 49–761.
Supekar, K., Musen, M., Menon, V., 2009. Development of large-scale functional brain networks in children. PLoS Biol. 7 (7), e1000157.
Supekar, K., Uddin, L.Q., Prater, K., Amin, H., Greicius, M.D., Menon, V., 2010. Development of functional and structural connectivity within the default mode network in young children. Neuroimage 52 (1), 290–301.
Tomasi, D., Volkow, N.D., 2012. Aging and functional brain networks. Mol. Psychiatry 17 (5), 549–558.
van den Heuvel, M.P., Sporns, O., 2011. Rich-club organization of the human connectome. J. Neurosci. 31 (44), 15775–15786.
Wang, L., Su, L., Shen, H., Hu, D., 2012. Decoding lifespan changes of the human brain using resting-state functional connectivity MRI. PLoS One 7 (8), e44530.
Wang, Z., Chen, L.M., Négyessy, L., Friedman, R.M., Mishra, A., Gore, J.C., Roe, A.W., 2013. The relationship of anatomical and functional connectivity to resting-state connectivity in primate somatosensory cortex. Neuron 78 (6), 1116–1126.
Yan, L., Zhuo, Y., Wang, B., Wang, D.J., 2011. Loss of coherence of low frequency fluctuations of BOLD fMRI in visual cortex of healthy aged subjects. Open Neuroimaging J. 5, 105–111.
Yan, C.G., Cheung, B., Kelly, C., Colcombe, S., Craddock, R.C., Di Martino, A., Li, Q., Zuo, X.N., Castellanos, F.X., Milham, M.P., 2013. A comprehensive assessment of regional variation in the impact of head movements on functional connectomics. Neuroimage 76 (1), 183–201.
Yang, Z., Chang, C., Xu, T., Jang, L., Handwerker, D.A., Castellanos, F.X., Milham, M.P., Bandettini, P.A., Zuo, X.N., 2014. Connectivity trajectory across lifespan differentiates the precuneus from the default network. Neuroimage 89, 45–56.
Yap, P.T., Fan, Y., Chen, Y., Gilmore, J.H., Lin, W., Shen, D., 2011. Development trends of white matter connectivity in the first years of life. PLoS One 6 (9), e24678.
Yeo, B.T.T., Krienen, F.M., Sepulcre, J., Sabuncu, M.R., Lashkari, D., Hollinshead, M., Roffman, J. L., Smoller, J.W., Zöllei, L., Polimeni, J.R., Fischl, B., Liu, H., Buckner, R.L., 2011. The organization of the human cerebral cortex estimated by intrinsic functional connectivity. J. Neurophysiol. 106 (3), 1125–1165.
Zhang, B., Horvath, S., 2005. A general framework for weighted gene co-expression network analysis. Stat. Appl. Genet. Mol. Biol. 4 (1), 1128.
Zuo, X.N., Kelly, C., Di Martino, A., Mennes, M., Margulies, D.S., Bangaru, S., Grzadzinski, R., Evans, A.C., Zang, Y.F., Castellanos, F.X., Milham, M.P., 2010. Growing together and growing apart: regional and sex differences in the lifespan developmental trajectories of functional homotopy. J. Neurosci. 30 (45), 15034–15043.
Zuo, X.N., Ehmke, R., Mennes, M., Imperati, D., Castellanos, F.X., Sporns, O., Milham, M.P., 2012. Network centrality in the human functional connectome. Cereb. Cortex 22 (8), 1862–1875.